



**HAL**  
open science

# Universal $G' \sim L^{-3}$ law for the low-frequency shear modulus of confined liquids

Alessio Zaccone, Laurence Noirez

► **To cite this version:**

Alessio Zaccone, Laurence Noirez. Universal  $G' \sim L^{-3}$  law for the low-frequency shear modulus of confined liquids. *Journal of Physical Chemistry Letters*, 2021, 12, pp.650-657. 10.1021/acs.jpcclett.0c02953 . hal-03105598v2

**HAL Id: hal-03105598**

**<https://hal.science/hal-03105598v2>**

Submitted on 4 Nov 2021

**HAL** is a multi-disciplinary open access archive for the deposit and dissemination of scientific research documents, whether they are published or not. The documents may come from teaching and research institutions in France or abroad, or from public or private research centers.

L'archive ouverte pluridisciplinaire **HAL**, est destinée au dépôt et à la diffusion de documents scientifiques de niveau recherche, publiés ou non, émanant des établissements d'enseignement et de recherche français ou étrangers, des laboratoires publics ou privés.

# 1 Universal $G' \sim L^{-3}$ Law for the Low-Frequency Shear Modulus of 2 Confined Liquids

3 Alessio Zaccone\* and Laurence Noirez\*



Cite This: <https://dx.doi.org/10.1021/acs.jpclett.0c02953>



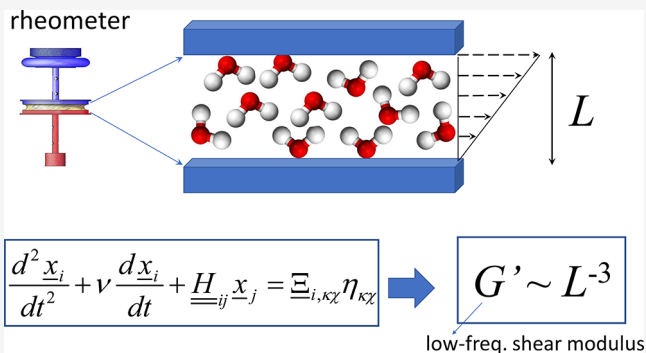
Read Online

ACCESS |

Metrics & More

Article Recommendations

4 **ABSTRACT:** Liquids confined to sub-millimeter scales have  
 5 remained poorly understood. One of the most striking effects is  
 6 the large elasticity revealed using good wetting conditions, which  
 7 grows upon further decreasing the confinement length,  $L$ . These  
 8 systems display a low-frequency shear modulus in the order of  $1-$   
 9  $10^3$  Pa, contrary to our everyday experience of liquids as bodies  
 10 with a zero low-frequency shear modulus. While early experimental  
 11 evidence of this effect was met with skepticism and abandoned,  
 12 further experimental results and, most recently, a new atomistic  
 13 theoretical framework have confirmed that liquids indeed possess a  
 14 finite low-frequency shear modulus  $G'$ , which scales with the  
 15 inverse cubic power of confinement length  $L$ . We show that this  
 16 law is universal and valid for a wide range of materials (liquid  
 17 water, glycerol, ionic liquids, non-entangled polymer liquids, isotropic liquids crystals). Open questions and potential applications in  
 18 microfluidics mechanochemistry, energy, and other fields are highlighted.



19 **O**ur daily life experience and education tell us that when a  
 20 liquid, e.g., liquid water, is subjected to an infinitesimal  
 21 shear stress, it flows. In physics, the absence of noticeable  
 22 mechanical resistance can be expressed by saying that the shear  
 23 elastic modulus  $G$  of liquids is exactly zero, where the shear  
 24 modulus represents the proportionality coefficient between the  
 25 applied shear stress ( $\sigma$ ) and the resulting deformation of a solid  
 26 body ( $\gamma$ ), i.e., Hooke's law,  $\sigma = G\gamma$ . Here, a first important  
 27 distinction comes into play, as the above statement is true for  
 28 nearly static measurements, i.e., at low frequency or low  
 29 deformation rate, where the shear modulus is zero, but at high  
 30 frequency or high rate of deformation the shear modulus of  
 31 liquids is large (as one would experience by diving into a  
 32 swimming pool from a considerable height, a possibly painful  
 33 experience if one is not an experienced diver!). This observation  
 34 reflects the fact that liquids at high frequency of external drive  
 35 behave like amorphous solids (e.g., glasses), because the atoms  
 36 or molecules are made to oscillate at such high speed by the  
 37 external field that they cannot escape the liquid cage made by  
 38 their nearest neighbors. This goes along with the ability of  
 39 liquids to sustain transverse acoustic waves at sufficiently high  
 40 momenta or high frequencies, as predicted in early work by  
 41 Yakov Frenkel in the 1940s.<sup>1</sup>

42 Besides this basic notion, which defines the essential property  
 43 of a liquid, our understanding of the physics of liquids is  
 44 incomplete.<sup>2</sup> This is due to the fact that atoms and molecules in a  
 45 liquid are in a state of disorder and random motions, which is  
 46 very different from atoms or molecules sitting on a regular lattice

in crystalline solids. Therefore, it is difficult to find a  
 47 mathematical description of the atomic or the molecular  
 48 dynamics in a liquid, from which quantitative explanations of  
 49 the macroscopic properties of liquids could be deduced.

50 As a consequence of this state of affairs, it has been impossible  
 51 so far to rationalize the mechanics of liquids on microscopic  
 52 scales. Already in 1989–1990, using the newly developed piezo-  
 53 quartz resonance device, it was experimentally observed that a  
 54 liquid film confined at a several micrometers scale exhibits an  
 55 unexpected shear elasticity at low frequency/rate of deformation,  
 56 a behavior much more akin to solids than to liquids.<sup>3,4</sup> In  
 57 spite of the fact that these experiments were led by Boris  
 58 Derjaguin, one of the most prominent Russian physico-chemists  
 59 of the 20th century, the observation was met with skepticism and  
 60 abandoned by the scientific community because of the  
 61 preconceived notion that liquids must have a zero shear  
 62 modulus. From the early 2000s, many other experiments  
 63 conducted by different teams across different length scales,  
 64 however, resulted in the same observation, extending the  
 65 identification of the “Derjaguin” shear elasticity up to the  
 66

Received: September 27, 2020

Accepted: December 23, 2020

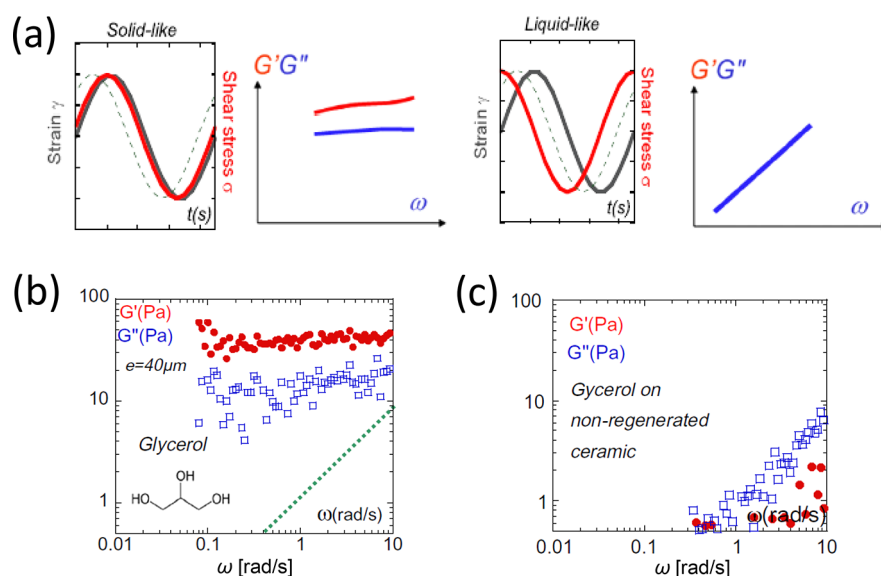


**Figure 1.** Dynamic viscoelastic response of liquids. Panel (a) shows a schematic depiction of time-dependent shear stress  $\sigma$  and shear strain  $\gamma$  for solid-like (left) and liquid-like (right) systems and the corresponding frequency-dependent viscoelastic curves. The lower set of figures shows the experimentally measured  $G'$  and  $G''$  as a function of oscillation frequency  $\omega$  for glycerol in good (cleaned/thermally regenerated ceramic), panel (b), and poor (non-cleaned ceramic), panel (c), surface-wetting conditions. The measurements are carried out at low gap thickness ( $e = 0.04$  mm) and at room temperature. Panel (b), obtained using a surface state perfectly free of impurities, displays higher viscoelastic moduli and leads to  $G' > G''$ , indicating a solid-like response. In panel (c), where the thermal regeneration of the surfaces has not been applied (hence causing a lower energy of adhesion, thus poor wetting and possibly de-wetting),  $G''$  scales exactly linear with  $\omega$ , in line with expectations for purely viscous liquids. Reproduced with permission from ref 19. Copyright 2010 Elsevier.

67 millimeter scale,<sup>5</sup> using different experimental techniques and  
 68 different liquids (from liquid water to liquid crystals to ionic  
 69 liquids and polymer melts).<sup>6–12</sup> A theoretical explanation for  
 70 these phenomena, however, has remained elusive (despite the  
 71 keen interest in this problem by Nobel laureate Pierre-Gilles de  
 72 Gennes, a former colleague of one of us, before his untimely  
 73 death in 2007).

74 In Figure 1 is shown the typical viscoelastic response of a sub-  
 75 millimeter confined liquid (glycerol at room temperature), in  
 76 terms of the storage shear modulus  $G'(\omega)$  and the dissipative  
 77 loss modulus  $G''(\omega)$ , which represent, respectively, the real and  
 78 imaginary parts of the complex shear modulus,  $G^* = G'(\omega) +$   
 79  $iG''(\omega)$ . Here,  $\omega$  is the frequency of the externally applied  
 80 mechanical oscillation field (oscillatory strain),  $\gamma = \gamma_0 \sin(\omega t)$ .  
 81 The shear strain  $\gamma$  is now time-dependent and triggers, under  
 82 conditions of the linear response, a stress response,  $\sigma = \sigma_0 \sin(\omega t$   
 83  $+ \delta)$ , where  $\delta$  is a phase which is  $\delta = 0$  for a perfectly elastic  
 84 response (Hooke's law) and  $\delta = \pi/2$  for a perfectly fluid  
 85 response. The situation is summarized in Figure 1a. Exper-  
 86 imentally, the solid-like response displays  $G' > G''$ , and a flat  
 87 plateau of  $G'$  at low frequency. The hallmark of a liquid-like  
 88 viscous response, instead, is that  $G' \ll G'' = \eta\omega$  (where  $\eta$  is the  
 89 shear viscosity) at low frequency. While bulk liquids have  $\delta = \pi/$   
 90  $2$  (perfectly viscous response) for low frequencies of oscillation  
 91 (in the range 0.001–10 Hz), liquids in confined geometry and/  
 92 or strongly in interaction with the substrate (wetting conditions)  
 93 may display  $\delta$  values much smaller than  $\pi/2$ , which indicates a  
 94 solid-like viscoelastic response. This goes along with a  
 95 substantial low-frequency plateau value of storage modulus,  $G'$   
 96  $> G''$ . An experimental example which illustrates the solid-like  
 97 response of confined liquids is provided in Figure 1b,c, showing  
 98 the mechanical response of a small-molecule liquid, glycerol, at  
 99 low frequency and room temperature. Among other simple  
 100 liquids, very similar mechanical responses at low frequency have

101 been measured for water,<sup>6</sup> for *o*-terphenyl (OTP),<sup>7</sup> and for ionic  
 102 liquids.<sup>8</sup> Similar solid-like properties have also been observed  
 103 with higher-molecular-weight liquids, such as linear alkanes,<sup>9</sup>  
 104 isotropic liquids crystals,<sup>10</sup> side-chain liquid crystals,<sup>11,12</sup>  
 105 entangled<sup>7</sup> and non-entangled polymers,<sup>10,13</sup> and supercooled  
 106 polypropylene glycol.<sup>14</sup> The same phenomena have also been  
 107 observed at the nanoscale in nano-confined liquids.<sup>15–18</sup>

108 It is important to note the role of boundary conditions, i.e., of  
 109 the surface energy. For certain solid surfaces in direct contact  
 110 with the liquid, the liquid molecules are firmly anchored to the  
 111 solid surface. This is typically associated with high wettability, or  
 112 good wetting, of the surface, and implies strong attractive  
 113 interactions between the liquid molecules and the surface. In  
 114 order to implement these conditions, therefore, it is also  
 115 necessary to consider the surface energy of the solid, in addition  
 116 to cleaned, atomically smooth conditions. If that is not the case,  
 117 e.g., for non-wetting surfaces, the liquid molecules in direct  
 118 contact with the surface are instead more free in their relative  
 119 motion with respect to the solid surface. This makes a big  
 120 difference in order to access the elastic response. It turns out  
 121 that, in the case of wetting surfaces, the mechanical response of  
 122 the confined liquid is higher and solid-like, whereas for non-  
 123 wetting surfaces, the standard purely viscous response is  
 124 observed. This phenomenon can be mechanistically explained  
 125 in terms of plane-wave null boundary conditions for the wetting  
 126 surfaces (or absence thereof, for non-wetting surfaces) in the  
 127 following theoretical analysis.

128 These experimental findings have recently been rationalized  
 129 from the point of view of theory. Theories of liquids have  
 130 normally focused on the high-frequency shear modulus for  
 131 which atomistic or molecular-level expressions are available,  
 132 such as the Zwanzig–Mountain formula,<sup>20</sup> precisely because the  
 133 low-frequency mechanical of bulk liquids was not supposed to  
 134 exist. In the allied field of amorphous solids, such as glasses,

135 instead, the mechanical response has been studied across the  
 136 entire frequency range, since amorphous solids obviously exhibit  
 137 a finite zero-frequency shear modulus. In particular, lattice  
 138 dynamics can be extended to deal with disordered systems  
 139 where the positions of atoms/molecules are completely random,  
 140 to arrive at theoretical expressions for the elastic constants and  
 141 for the viscoelastic moduli.<sup>21</sup> The resulting theoretical frame-  
 142 work is sometimes referred to as non-affine lattice dynamics, or  
 143 NALD.<sup>22,23</sup> The theory has proved effective in quantitatively  
 144 describing elastic, viscoelastic, and plastic responses of systems  
 145 as diverse as jammed random packings and random networks,<sup>21</sup>  
 146 glassy polymers,<sup>24–26</sup> metallic glass,<sup>27</sup> and colloidal glasses.<sup>28</sup>  
 147 Furthermore, NALD intrinsically takes into account long-range  
 148 correlation phenomena<sup>29,30</sup> that are present also in liquids and  
 149 give rise to acoustic wave propagation.

150 The usual starting point is the equation of motion of a  
 151 microscopic building block, i.e., an atom or a molecule for  
 152 atomic liquids or molecular liquids, respectively. In the case of  
 153 polymers, the building block could be identified with a monomer  
 154 of the polymer chain.<sup>24</sup> Following previous literature,<sup>21,22</sup> we  
 155 introduce the Hessian matrix of the system  $\underline{\underline{H}}_{ij} = -\partial^2 \mathcal{U} / \partial \underline{\underline{q}}_i \partial \underline{\underline{q}}_j$ ,  
 156 where  $\mathcal{U}$  is the internal energy, and the affine force field  $\underline{\Xi}_{i,\kappa\chi} =$   
 157  $\partial \underline{f}_i / \partial \eta_{\kappa\chi}$ , where  $\eta_{\kappa\chi}$  is the strain tensor. For example, for simple  
 158 shear deformation the  $xy$  entry of tensor  $\eta_{\kappa\chi}$  is given by a scalar  $\gamma$ ,  
 159 i.e., the shear strain introduced above, which coincides with the  
 160 angle of deformation.

161 Furthermore,  $\underline{\underline{q}}_i$  is the coordinate of atom  $i$  in the initial un-  
 162 deformed frame (denoted with the ring notation), while  $\underline{f}_i =$   
 163  $\partial \mathcal{U} / \partial \underline{q}_i$  denotes the force acting on atom  $i$  in the affine position,  
 164 i.e., in the initial frame acted upon by the macroscopic  
 165 deformation, hence the name “affine” force-field. See Figure 2a  
 166 for a visual representation of affine positions in a deformed  
 167 frame. Greek indices refer to Cartesian components of the  
 168 macroscopic deformation (e.g.,  $\kappa\chi = xy$  for shear). For liquids  
 169 (and to a lesser extent, also for glasses<sup>24</sup>), the Hessian  $\underline{\underline{H}}_{ij}$  is  
 170 normally evaluated in a reference state obtained from averaging  
 171 over MD configurations to include instantaneous normal modes,  
 172 or INMs (purely imaginary vibrational frequencies).<sup>24</sup> For more  
 173 details about INMs, see ref 31.

174 As shown in previous works, the equation of motion of atom  $i$   
 175 in a disordered medium subjected to an external small amplitude  
 176 strain, in mass-rescaled coordinates, can be written as  
 177 follows:<sup>22,24</sup>

$$178 \quad \frac{d^2 \underline{x}_i}{dt^2} + \nu \frac{d \underline{x}_i}{dt} + \underline{\underline{H}}_{ij} \underline{x}_j = \underline{\Xi}_{i,\kappa\chi} \eta_{\kappa\chi} \quad (1)$$

179 where the summation convention is operative for both Latin and  
 180 Greek indices. Also,  $\eta_{\kappa\chi}$  are the components of the Green–Saint  
 181 Venant strain tensor, and  $\nu$  is a microscopic friction coefficient  
 182 which arises from long-range dynamical coupling between atoms  
 183 mediated by anharmonicity of the pair potential. The term on  
 184 the right-hand side physically represents the effect of the  
 185 disordered (non-centrosymmetric) environment leading to  
 186 non-affine motions: a net force acts on atom  $i$  in the affine  
 187 position (i.e., the position prescribed by the external strain  
 188 tensor  $\eta_{\kappa\chi}$ ). The situation is schematically depicted in Figure 2b,  
 189 which contrasts a centrosymmetric environment (left panel),  
 190 where all atoms are at mechanical equilibrium, even in the affine  
 191 position (here for an infinitesimal strain), due to cancellation of  
 192 nearest-neighbor forces that are mirror-images of each other

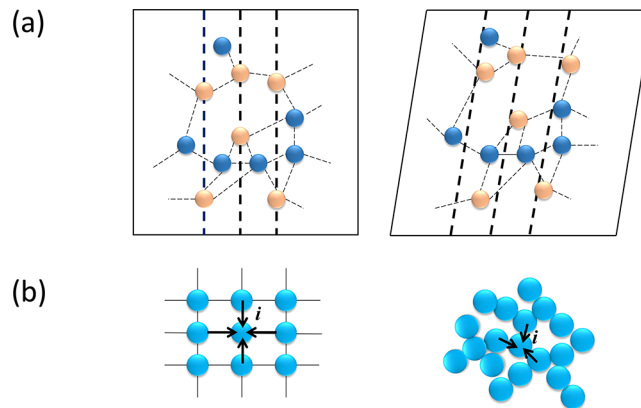


**Figure 2.** Schematic illustration of non-affine displacements in amorphous media. Panel (a) shows the rearrangements or displacements of atoms upon application of an external shear strain. If the deformation were affine, atoms which sit exactly on the dashed lines in the un-deformed frame (left) would still sit exactly on dashed lines also in the deformed frame (right). However, in a disordered environment this does not happen, and in the deformed frame the atoms that were sitting on the dashed lines in the un-deformed frame are no longer sitting on the dashed lines, but are displaced from them. The distance from the actual positions of the atoms to the dashed line corresponds to the non-affine displacements. Panel (b) provides a visual explanation of the origin of non-affine displacements in disordered environments. The left figure shows a perfect lattice where, upon applying a small deformation, the nearest-neighbor forces from surrounding atoms cancel each other out in the affine positions, so there is no need for non-affine displacements to arise. In the right figure, instead, the tagged atom  $i$  is not a center of inversion symmetry, which implies that nearest-neighbor forces from surrounding atoms do not balance in the affine position, and hence a net force arises which triggers the non-affine displacement in order to maintain mechanical equilibrium.

193 across the central particle, with the situation in a disordered  
 194 system (liquid or amorphous solid, right panel). In the latter  
 195 case, the nearest-neighbor forces do not cancel, thus leading to a  
 196 net force acting on the central atom.

197 As a consequence, in order to keep mechanical equilibrium on  
 198 all atoms throughout the deformation, an additional *non-affine*  
 199 displacement is required in order to relax the force  $f_i$  acting in the  
 200 affine position. This displacement brings each atom  $i$  to a new  
 201 (non-affine) position. A schematic depiction of a non-affine  
 202 displacement is shown in Figure 2a.

203 The equation of motion eq 1 can also be derived from first-  
 204 principles, from a model particle-bath Hamiltonian as shown in  
 205 previous work.<sup>24</sup> Using standard manipulations (Fourier  
 206 transformation and eigenmode decomposition from time to  
 207 eigenfrequency<sup>22</sup>), and applying the definition of mechanical  
 208 stress, we obtain the following expression for the viscoelastic  
 209 (complex) elastic constants:<sup>22,24</sup>

$$210 \quad C_{\alpha\beta\kappa\chi}(\omega) = C_{\alpha\beta\kappa\chi}^{\text{Born}} - \frac{1}{V} \sum_n \frac{\hat{\Xi}_{n,\alpha\beta} \hat{\Xi}_{n,\kappa\chi}}{\omega_{p,n}^2 - \omega^2 + i\omega\nu} \quad (2)$$

211 where  $C_{\alpha\beta\kappa\chi}^{\text{Born}}$  is the Born or affine part of the elastic constant, i.e.,  
 212 what survives in the high-frequency limit. Here,  $\omega$  represents the  
 213 oscillation frequency of the external strain field, whereas  $\omega_p$   
 214 denotes the internal eigenfrequency of the liquid (which results,  
 215 e.g., from diagonalization of the Hessian matrix<sup>24</sup>). We use the  
 216 notation  $\omega_p$  to differentiate the eigenfrequency from the external  
 217 oscillation frequency  $\omega$ .

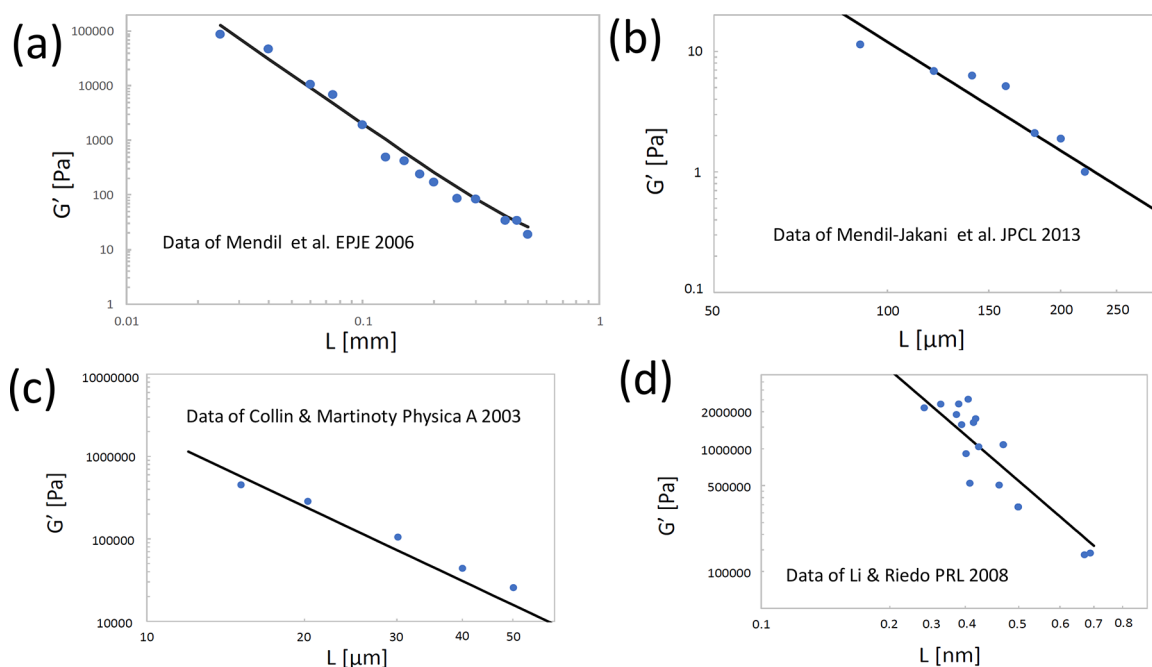


**Figure 3.** Experimental data of low-frequency shear modulus  $G'$  versus confinement length  $L$  for different systems, where circles represent experimental data while the solid line is the law  $G' \sim L^{-3}$  derived in ref 37. Panel (a) shows the comparison for PAOCH<sub>3</sub>, an isotropic liquid crystal system from ref 10; (b) shows the same comparison for ionic liquids, from ref 8; (c) shows experimental data for short-chain (non-entangled) polystyrene melts from ref 13; and (d) shows experimental data for nanoconfined water from ref 15.

218 As already mentioned above, an atomistic expression for  $G_\infty \equiv$   
 219  $C_{\alpha\beta\gamma\chi}^{\text{Born}}$  is provided by the well-known Zwanzig–Mountain  
 220 formula,<sup>20</sup> in terms of the pair potential  $V(r)$  and the radial  
 221 distribution function  $g(r)$ . The sum over  $n$  in eq 2 runs over all  
 222  $3N$  degrees of freedom (given by the atomic or molecular  
 223 building blocks with central-force interactions). Also, we  
 224 recognize the typical form of a Green's function, with an  
 225 imaginary part given by damping and poles  $\omega_{p,n}$  that correspond  
 226 to the eigenfrequencies of the excitations.

227 At this point we use a key assumption of plane waves; i.e., we  
 228 assume that, at low values of wavenumber  $k$  (i.e., for long  
 229 wavelengths  $\lambda$ ), liquids can support shear elastic waves.  
 230 Propagation of longitudinal acoustic waves in liquids is, of  
 231 course, a well-known fact to everyone who does snorkeling or  
 232 swims under the water level, with firmly established  
 233 experimental and theoretical evidence of longitudinal acoustic  
 234 dispersion relations.<sup>32–34</sup> For transverse or shear acoustic waves

235 in liquids, instead, there is no propagation below a characteristic  
 236 wavenumber. Indeed, there is an onset value of  $k$ , that we shall  
 237 denote  $k_g$ , above which these modes can propagate in liquids,  
 238 known as the  $k$ -gap,<sup>2</sup> again a result due originally to Frenkel,<sup>1</sup>  
 239 and recently demonstrated by Trachenko and co-workers.<sup>35,36</sup>

240 Following the analytical steps presented in ref 37, we arrive at  
 241 the following expression for the complex shear modulus:

$$G^*(\omega) = G_\infty - B \int_{1/L}^{k_D} \frac{\omega_{p,L}^2(k)}{\omega_{p,L}^2(k) - \omega^2 + i\omega\nu} k^2 dk - B \int_{k_{\min}}^{k_D} \frac{\omega_{p,T}^2(k)}{\omega_{p,T}^2(k) - \omega^2 + i\omega\nu} k^2 dk \quad (3)$$

243 where the first integral represents the non-affine (negative or  
 244 softening) contribution due to longitudinal (L) acoustic modes,  
 245 while the second integral represents the non-affine (also  
 246 softening) contribution due to the transverse (T) acoustic

247 modes. The upper integration limit in the  $k$  integrals is set, as  
 248 usual, by the Debye wavenumber  $k_D$ . In the above expression,  $k_{\min} = \max(k_g, \frac{1}{L})$  is an “infrared” cutoff for the transverse  
 249 modes, with  $k_g$  the onset wavenumber for transverse phonons in  
 250 liquids (the  $k$ -gap) and  $L$  the confinement length along the  $z$   
 251 direction. In the above treatment, dealing with plane waves in  
 252 3D implies the condition  $\sqrt{k_x^2 + k_y^2 + k_z^2} = k = 2\pi/\lambda$ , which  
 253 leads to the spherical integrals of eq 3, with the metric factor  $k^2$ .  
 254

255 For the longitudinal modes, one can resort to the Hubbard–  
 256 Beeby theory of collective longitudinal modes in liquids,<sup>32</sup> which  
 257 has been shown to provide a good description of experimental  
 258 data, and thus use eq 43 from ref 32 for  $\omega_{p,L}(k)$  inside the  
 259 integral above. As shown in ref 37, the final result for the low-  
 260 frequency  $G'$  does not depend on the form of the  $\omega_{p,L}(k)$   
 261 dispersion relation. However, for the mathematical complete-  
 262 ness of the theory, it is important to specify which analytical  
 263 forms for the dispersion relations can be used.

264 Anyway, upon taking the real part of  $G^*$ , which gives the  
 265 storage modulus  $G'$ , and focusing on low external oscillation  
 266 frequencies  $\omega \ll \omega_p$  used experimentally, in both integrals the  
 267 numerator and denominator cancel out, leaving the same  
 268 expression in both integrals. Therefore, as anticipated above, the  
 269 final low-frequency result does not depend on the actual form of  
 270  $\omega_{p,L}(k)$ , nor of  $\omega_{p,T}(k)$ , although the latter, due to the  $k$ -gap,  
 271 plays an important role (see the expression for  $k_{\min}$  above) in  
 272 controlling the “infrared” cutoff of the transverse integral.  
 273 In the experiments where the size effect of confinement is seen,  
 274  $k_g \ll \frac{1}{L}$ ,<sup>38</sup> and  $k_{\min} = \frac{1}{L}$ , thus leading to

$$G' = G_\infty - \alpha \int_{1/L}^{k_D} k^2 dk = G_\infty - \frac{\alpha}{3} k_D^3 + \frac{\beta}{3} L^{-3} \quad (4)$$

275 For the lower limit of the non-affine integral, we used an  
 276 “infrared” cutoff,  
 277

$$k_{\min} \equiv |\mathbf{k}_{\min}| = 2\pi\sqrt{(1/L_x)^2 + (1/L_y)^2 + (1/L)^2} \quad (5)$$

by assuming that the liquid is confined along the  $z$  direction, such that  $L \equiv L_z \ll L_x, L_y$ ; the lower limit in the non-affine integral over  $k$ -space thus reduces to  $1/L$ , as displayed in eq 4. A rigorous estimate of the  $k$ -integral in eq 4, including exact prefactors, can be found in ref 39.

In eq 4, the only term which depends on the system size is the last term, while  $\alpha$  and  $\beta$  are numerical prefactors. In liquids that are in thermodynamic equilibrium and for quasistatic deformations, a different version of the non-affine response formalism called the stress-fluctuation formalism can be used. It has been rigorously demonstrated that the two versions of the formalism are equivalent in ref 40. Using the stress-fluctuation non-affine formalism in combination with standard equilibrium statistical mechanics, it has been shown in ref 41 that the affine or high-frequency (Born) term  $G_\infty$  and the negative non-affine term (here,  $-\frac{\alpha}{3}k_D^3$ ) cancel each other out exactly, such that  $G'(\omega \rightarrow 0) = 0$  for  $L \rightarrow \infty$  (bulk liquids). Therefore, for liquids under sub-millimeter confinement, only the third term in the above equation survives, and we finally obtain

$$G' \approx \beta' L^{-3} \quad (6)$$

where  $\beta' = \beta/3$  is a numerical prefactor. This law was derived for the first time in ref 37. It is worth noticing that  $G_\infty$  is independent of  $L$ . This fact can be seen, e.g., through the Zwanzig–Mountain formula, where the main contribution to  $G_\infty$  is given as an integral that contains  $dV(r)/dr$  as a multiplying factor in the integrand, with  $dV(r)/dr = 0$  after a few molecular diameters. This, in turn, implies that no dependencies on length scales much larger than the nearest-neighbor cage can be present in  $G_\infty$ .

The above theory clarifies that the liquid confinement between two plates is able to “remove” certain low-frequency normal-mode collective oscillations of molecules, associated with the non-affine motions (i.e., negative contributions to the elasticity), which are responsible for the fluid response of liquids under standard macroscopic (“unconfined”) conditions. These motions are responsible for reducing the shear modulus basically to zero in macroscopic bulk liquids. Under confinement, instead, the shear modulus is non-zero because these collective oscillations modes are suppressed, and the theory of Zaccone and Trachenko<sup>37</sup> provides the universal law by which the shear modulus grows upon reducing the confinement (gap) size. In particular, the static shear modulus grows with the inverse cubic power of the gap size.

In ref 37, the law  $G' \sim L^{-3}$  was found to provide a perfect description of experimental data measured in an isotropic liquid crystal system (PAOCH<sub>3</sub>) upon varying the confinement length using a conventional rheometer. Here, we show that this law appears to be truly universal, and we present theoretical fittings of several, very different systems in Figure 3.

In all these systems, i.e., polymer melts of relatively low molecular weight, isotropic liquid crystals, ionic liquids, and even nano-confined water, the law eq 6 appears robust, as shown in Figure 3. In the case of nano-confined water,<sup>15</sup> one would expect a crossover from  $\sim L^{-3}$  into an  $L^{-1}$  regime once a 2D monolayer is reached. This is expected because the  $k$ -space integral in eq 4 contains a metric factor  $k$  in 2D, instead of  $k^2$  for 3D (in fact,  $k^{d-1}$  for generic  $d$ -dimensional space). This crossover is not seen in the data of Figure 3d, which calls for further investigations, both experimentally and theoretically.

Experimental data have also been reported for OTP, an organic liquid (data not shown here).<sup>7</sup> Those data also show the  $\sim L^{-3}$  behavior, but the data at the shortest confinement length,  $\sim 0.01$  mm, suggest the possible existence of a plateau upon going toward lower  $L$ , while the experimental accuracy is lowered as the confinement increases. The paucity of experimental data does not allow for drawing a definitive conclusion on this effect (i.e., the possible existence of a plateau in  $G'$  at low  $L$  in certain systems), which should also be the object of further investigation, both experimentally and in theory.

As mentioned earlier, a crucial role is played by the surface anchoring. The solid-like response of confined liquids is indeed observed mainly for atomically smooth surfaces (crystal planes) or for conditions of good wetting between liquid and solid surfaces (high energy surfaces). Instead, a standard, purely viscous response is reported for non-wetting or poorly wetting surfaces; see Figure 4 for a schematic illustration of two different

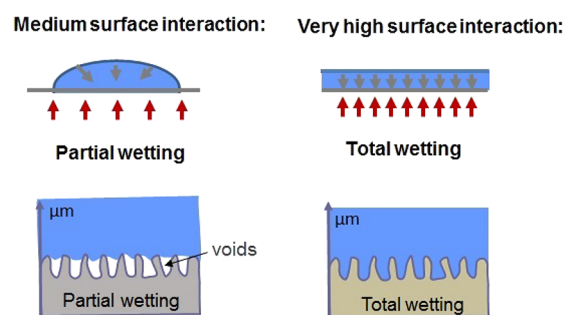


**Figure 4.** Schematic illustration of different levels of surface interaction between liquid molecules and solid substrate. A not-so-strong attractive interaction leads to partial wetting (left panel), whereas a strong attractive interaction with the solid surface leads to total wetting filling in the rough edges (right panel).

surface wetting conditions. The same observation has been made in the case of nanoconfined water, with a substantially higher viscosity measured in the case of good wetting in ref 16.

From the theoretical point of view, this fact can be explained by referring to the non-affine lattice dynamic framework summarized above. In particular, wettability connects with the assumption of plane waves and with the implicit *null boundary conditions* for the displacement field of plane waves. This leads straightforward to the term  $\sim L^{-3}$  in eq 4 above, which is the term responsible for the solid-like elastic response. Without the full wetting boundary conditions between the liquid and the solid surface, the liquid molecules would not be well-anchored to the solid surface, so the null boundary condition for the acoustic waves would not apply, and the very existence of elastic plane waves would then be called into question. Certainly, the above theoretical framework would not be applicable in that case, as it relies on the ability of the liquid to support plane waves. We can speculate that, when molecules are not anchored to the solid surface, the effective “removal” of softening non-affine motions during the displacement and due to confinement is less effective; hence, the rigidifying effect of “cutting” non-affine motions off due to confinement during the deformation, would not be active. A more precise explanation may require a different theoretical approach, possibly working in eigenfrequency domain rather than in  $k$ -space, and is an interesting problem for future research.

Finally, it is important to point out that the non-zero low-frequency shear elasticity has been measured in various liquids irrespective of their surface tension (alkanes, ionic liquids, and

383 polymer melts typically exhibit low surface tension). Since the  
384 interfacial (air/liquid) energy scales as the inverse of the surface,  
385 significant contributions to  $G'$  would be possible if the sample  
386 area changes drastically during the oscillatory shear. Bad filling,  
387 bad wetting, and large-amplitude oscillator strain (LAOS)  
388 conditions could produce a weak “false” torque by breaking the  
389 rotational symmetry in the plane.<sup>42</sup> In contrast, the genuine low-  
390 frequency shear elasticity intrinsic to the confined liquid state is  
391 accessible under conditions where the above artifacts are  
392 carefully avoided, and by ensuring a good wetting and low  
393 strain—that is, as close as possible to the equilibrium conditions.  
394  $G'$  then vanishes by increasing the shear strain (at low gap) to  
395 make room for the conventional viscous or viscoplastic flow  
396 behavior, which could be understood as the non-linear evolution  
397 of the finite low-frequency shear elasticity,<sup>3–7</sup> similar to what  
398 happens in amorphous solids upon crossing the yielding/  
399 plasticity transition.<sup>27,28</sup>

400 A number of outstanding questions remain open for future  
401 investigations. For example, it could be interesting to explore  
402 what kind of connection exists between the above scenario of  
403 solid-like elasticity of confined liquids and the glass transition  
404 under confinement. The latter is an intensively studied problem,  
405 especially in the context of thin polymer films.<sup>43,44</sup> Another  
406 important issue is the progress that can be made with numerical  
407 simulations. In molecular dynamics (MD), the shear modulus of  
408 a confined liquid can be measured, but the noise is currently too  
409 large (since the size of MD-simulated systems is small) to make  
410 predictions for most realistic situations.<sup>45</sup> Another issue is  
411 represented by the small time step used, especially in atomistic  
412 simulations (on the order of femtoseconds), which prevents  
413 accessing the low-frequency shear modulus. Quasi-static  
414 deformation methods implemented atomistically could be a  
415 step forward, but they have not demonstrated quantitative  
416 predictive power thus far, in comparison with experiments. Also,  
417 the power-law nature of the relation  $G' \sim L^{-3}$  implies the  
418 absence of characteristic length scales (as is typical for power-  
419 laws), which suggests that the same mechanisms apply at  
420 different length scales; i.e., the same laws apply with  $L$  being on  
421 the sub-millimeter, micrometer, or nanometer scale. Similarities  
422 between trends observed for sub-millimeter<sup>10</sup> and nano-  
423 confined fluids,<sup>15,16</sup> in terms of both solid-like mechanical  
424 properties and role of wetting,<sup>46</sup> suggest that this may indeed be  
425 the case, but further research is required to more firmly establish  
426 a complete multi-scale framework.

427 The potential applications of solid-like elasticity of confined  
428 liquids, and its tunability via the control and modulation of the  
429 interfacial energy and gap size  $L$ , are manifold, encompassing  
430 fields as diverse as mechanical stress-assisted manipulation of  
431 soft and biological matter in microfluidics,<sup>47–49</sup> protective  
432 equipment,<sup>50</sup> biomedical flow applications,<sup>51</sup> oil recovery,<sup>52</sup>  
433 heat transfer in liquids,<sup>53</sup> and phase transitions under confine-  
434 ment.<sup>54</sup> Recently, it has been demonstrated that the thermal  
435 response of confined liquids is very similar to that of solids,<sup>55</sup>  
436 which opens up new opportunities for exploiting thermo-  
437 elasticity of confined fluids, e.g., for energy conversion.

438 Finally, another potential exciting application of this effect is  
439 in the emerging fields of mechanochemistry<sup>56–59</sup> and  
440 mechanobiology:<sup>60</sup> a (confined) liquid with a finite low-  
441 frequency shear modulus  $G'$  is able to support mechanical  
442 stress-transmission much more efficiently and with much lower  
443 dissipative losses compared to standard viscous liquids. This fact  
444 may open up new avenues for mechanically induced enhance-  
445 ment of chemical reaction kinetics, by combining the force-

transmission efficiency typical of elastic solids with all the  
favorable solvation and solubility properties of liquids.<sup>61–64</sup>

## AUTHOR INFORMATION

### Corresponding Authors

Alessio Zaccone – Department of Physics “A. Pontremoli”,  
University of Milan, 20133 Milan, Italy; Department of  
Chemical Engineering and Biotechnology and Cavendish  
Laboratory, University of Cambridge, CB30AS Cambridge,  
U.K.; [orcid.org/0000-0002-6673-7043](https://orcid.org/0000-0002-6673-7043);  
Email: [alessio.zaccone@unimi.it](mailto:alessio.zaccone@unimi.it)

Laurence Noirez – Laboratoire Léon Brillouin (CEA-CNRS),  
Université Paris-Saclay, CEA-Saclay, 91191 Gif-sur-Yvette,  
France; Email: [laurence.noirez@cea.fr](mailto:laurence.noirez@cea.fr)

Complete contact information is available at:

<https://pubs.acs.org/10.1021/acs.jpcllett.0c02953>

### Notes

The authors declare no competing financial interest.

### Biographies

Alessio Zaccone

Laurence Noirez

## ACKNOWLEDGMENTS

A.Z. thanks Kostya Trachenko and Ivan Kriuchevskiy for  
enlightening discussions. A.Z. acknowledges financial support  
from the U.S. Army Research Office, grant no. W911NF-19-2-  
0055. L.N. expresses her gratitude to the late P.-G. de Gennes  
and wishes to acknowledge F. Volino for discussions about non-  
extensive viscoelastic properties.

## REFERENCES

- (1) Frenkel, J. *Kinetic Theory of Liquids*; Oxford University Press, Oxford, 1946.
- (2) Trachenko, K.; Brazhkin, V. V. Collective modes and thermodynamics of the liquid state. *Rep. Prog. Phys.* **2016**, *79*, 016502.
- (3) Derjaguin, B.; Bazaron, U.; Zandanova, K.; Budaev, O. The complex shear modulus of polymeric and small-molecule liquids. *Polymer* **1989**, *30*, 97–103.
- (4) Derjaguin, B. V.; Bazaron, U. B.; Lamazhapova, K. D.; Tsidyrov, B. D. Shear elasticity of low-viscosity liquids at low frequencies. *Phys. Rev. A: At, Mol, Opt. Phys.* **1990**, *42*, 2255–2258.
- (5) Noirez, L. Origin of shear-induced phase transitions in melts of liquid-crystal polymers. *Phys. Rev. E* **2005**, *72*, 051701.
- (6) Noirez, L.; Baroni, P. Identification of a low-frequency elastic behaviour in liquid water. *J. Phys.: Condens. Matter* **2012**, *24*, 372101.
- (7) Noirez, L.; Mendil-Jakani, H.; Baroni, P. Identification of finite shear-elasticity in the liquid state of molecular and polymeric glass-formers. *Philos. Mag.* **2011**, *91*, 1977–1986.
- (8) Mendil-Jakani, H.; Baroni, P.; Noirez, L.; Chancelier, L.; Gebel, G. Highlighting a Solid-Like Behavior in Tri-octylmethylammonium Bis(trifluoromethanesulfonyl)imide. *J. Phys. Chem. Lett.* **2013**, *4*, 3775–3778.
- (9) Noirez, L.; Baroni, P.; Cao, H. Identification of Shear Elasticity at Low Frequency in Liquid n-Heptadecane, Liquid Water and RT-Ionic Liquids [emim][Tf2N]. *J. Mol. Liq.* **2012**, *176*, 71–75 (Special Issue on Dynamics and Phase Transition: Selected Papers on Molecular Liquids presented at the EMLG/JMLG 2011 Annual Meeting 11–15 September 2011).
- (10) Mendil, H.; Baroni, P.; Noirez, L. Solid-like rheological response of non-entangled polymers in the molten state. *Eur. Phys. J. E: Soft Matter Biol. Phys.* **2006**, *19*, 77–85.

- 504 (11) Gallani, J. L.; Hilliou, L.; Martinoty, P.; Keller, P. Abnormal  
505 viscoelastic behavior of side-chain liquid-crystal polymers. *Phys. Rev.*  
506 *Lett.* **1994**, *72*, 2109–2112.
- 507 (12) Martinoty, P.; Hilliou, L.; Mauzac, M.; Benguigui, L.; Collin, D.  
508 Side-Chain Liquid-Crystal Polymers: Gel-like Behavior below Their  
509 Gelation Points. *Macromolecules* **1999**, *32*, 1746–1752.
- 510 (13) Collin, D.; Martinoty, P. Dynamic macroscopic heterogeneities  
511 in a flexible linear polymer melt. *Phys. A* **2003**, *320*, 235–248.
- 512 (14) Chushkin, Y.; Caronna, C.; Madsen, A. Low-frequency elastic  
513 behavior of a supercooled liquid. *EPL (Europhysics Letters)* **2008**, *83*,  
514 36001.
- 515 (15) Li, T.-D.; Riedo, E. Nonlinear Viscoelastic Dynamics of  
516 Nanoconfined Wetting Liquids. *Phys. Rev. Lett.* **2008**, *100*, 106102.
- 517 (16) Ortiz-Young, D.; Chiu, H.-C.; Kim, S.; Voitchovsky, K.; Riedo, E.  
518 The interplay between apparent viscosity and wettability in nano-  
519 confined water. *Nat. Commun.* **2013**, *4*, 2482.
- 520 (17) Monet, G.; Paineau, E.; Chai, Z.; Amara, M. S.; Orecchini, A.;  
521 Jimenez-Ruiz, M.; Ruiz-Caridad, A.; Fine, L.; Rouzière, S.; Liu, L.-M.;  
522 Teobaldi, G.; Rols, S.; Launois, P. Solid wetting-layers in inorganic  
523 nano-reactors: the water in imogolite nanotube case. *Nanoscale Adv.*  
524 **2020**, *2*, 1869–1877.
- 525 (18) Ito, K.; Faraone, A.; Tyagi, M.; Yamaguchi, T.; Chen, S.-H.  
526 Nanoscale dynamics of water confined in ordered mesoporous carbon.  
527 *Phys. Chem. Chem. Phys.* **2019**, *21*, 8517–8528.
- 528 (19) Noirez, L.; Baroni, P. Revealing the solid-like nature of glycerol at  
529 ambient temperature. *J. Mol. Struct.* **2010**, *972*, 16–21 (Horizons in  
530 hydrogen bond research 2009).
- 531 (20) Zwanzig, R.; Mountain, R. D. High-frequency elastic moduli of  
532 simple fluids. *J. Chem. Phys.* **1965**, *43*, 4464–4471.
- 533 (21) Zacccone, A.; Scossa-Romano, E. Approximate analytical  
534 description of the nonaffine response of amorphous solids. *Phys. Rev.*  
535 *B: Condens. Matter Mater. Phys.* **2011**, *83*, 184205.
- 536 (22) Lemaitre, A.; Maloney, C. Sum Rules for the Quasi-Static and  
537 Visco-Elastic Response of Disordered Solids at Zero Temperature. *J.*  
538 *Stat. Phys.* **2006**, *123*, 415.
- 539 (23) Zacccone, A. Elastic Deformations in Covalent Amorphous Solids.  
540 *Mod. Phys. Lett. B* **2013**, *27*, 1330002.
- 541 (24) Palyulin, V. V.; Ness, C.; Milkus, R.; Elder, R. M.; Sirk, T. W.;  
542 Zacccone, A. Parameter-free predictions of the viscoelastic response of  
543 glassy polymers from non-affine lattice dynamics. *Soft Matter* **2018**, *14*,  
544 8475–8482.
- 545 (25) Ness, C.; Palyulin, V. V.; Milkus, R.; Elder, R.; Sirk, T.; Zacccone,  
546 A. Nonmonotonic dependence of polymer-glass mechanical response  
547 on chain bending stiffness. *Phys. Rev. E: Stat. Phys., Plasmas, Fluids,*  
548 *Relat. Interdiscip. Top.* **2017**, *96*, 030501.
- 549 (26) Elder, R. M.; Zacccone, A.; Sirk, T. W. Identifying Nonaffine  
550 Softening Modes in Glassy Polymer Networks: A Pathway to Chemical  
551 Design. *ACS Macro Lett.* **2019**, *8*, 1160–1165.
- 552 (27) Zacccone, A.; Schall, P.; Terentjev, E. M. Microscopic origin of  
553 nonlinear nonaffine deformation in bulk metallic glasses. *Phys. Rev. B:*  
554 *Condens. Matter Mater. Phys.* **2014**, *90*, 140203.
- 555 (28) Laurati, M.; Maßhoff, P.; Mutch, K. J.; Egelhaaf, S. U.; Zacccone,  
556 A. Long-Lived Neighbors Determine the Rheological Response of  
557 Glasses. *Phys. Rev. Lett.* **2017**, *118*, 018002.
- 558 (29) Shelton, D. P. Long-range orientation correlation in water. *J.*  
559 *Chem. Phys.* **2014**, *141*, 224506.
- 560 (30) Zhang, Z.; Kob, W. Revealing the three-dimensional structure of  
561 liquids using four-point correlation functions. *Proc. Natl. Acad. Sci. U. S.*  
562 *A.* **2020**, *117*, 14032–14037.
- 563 (31) Strat, R. M. The Instantaneous Normal Modes of Liquids. *Acc.*  
564 *Chem. Res.* **1995**, *28*, 201–207.
- 565 (32) Hubbard, J.; Beeby, J. L. Collective motion in liquids. *J. Phys. C:*  
566 *Solid State Phys.* **1969**, *2*, 556–571.
- 567 (33) Takeno, S.; Goda, M. A Theory of Phonon-Like Excitations in  
568 Non-Crystalline Solids and Liquids. *Prog. Theor. Phys.* **1972**, *47*, 790–  
569 806.
- 570 (34) Hansen, J.-P.; McDonald, I. R. *Theory of Simple Liquids*; Elsevier,  
571 Amsterdam, 2013.
- (35) Yang, C.; Dove, M. T.; Brazhkin, V. V.; Trachenko, K. Emergence  
572 and Evolution of the  $k$  Gap in Spectra of Liquid and Supercritical States. *Phys. Rev. Lett.* **2017**, *118*, 215502. 573
- (36) Khusnutdinoff, R. M.; Cockrell, C.; Dicks, O. A.; Jensen, A. C. S.;  
574 Le, M. D.; Wang, L.; Dove, M. T.; Mokshin, A. V.; Brazhkin, V. V.;  
575 Trachenko, K. Collective modes and gapped momentum states in liquid  
576 Ga: Experiment, theory, and simulation. *Phys. Rev. B: Condens. Matter*  
577 *Mater. Phys.* **2020**, *101*, 214312. 578
- (37) Zacccone, A.; Trachenko, K. Explaining the low-frequency shear  
579 elasticity of confined liquids. *Proc. Natl. Acad. Sci. U. S. A.* **2020**, *117*,  
580 19653–19655. 581
- (38) Jackson, J. K.; De Rosa, M. E.; Winter, H. H. Molecular Weight  
582 Dependence of Relaxation Time Spectra for the Entanglement and  
583 Flow Behavior of Monodisperse Linear Flexible Polymers. *Macro-*  
584 *molecules* **1994**, *27*, 2426–2431. 585
- (39) Phillips, A. E.; Baggioni, M.; Sirk, T. W.; Trachenko, K.; Zacccone,  
586 A. Universal  $L^{-3}$  finite-size effects in the viscoelasticity of confined  
587 amorphous systems. *arXiv e-Prints* **2020**, No. arXiv:2012.05149[cond-  
588 mat.soft]. 589
- (40) Mizuno, H.; Silbert, L. E.; Sperl, M.; Mossa, S.; Barrat, J.-L.  
590 Cutoff nonlinearities in the low-temperature vibrations of glasses and  
591 crystals. *Phys. Rev. E: Stat. Phys., Plasmas, Fluids, Relat. Interdiscip. Top.*  
592 **2016**, *93*, 043314. 593
- (41) Wittmer, J. P.; Xu, H.; Polińska, P.; Weysser, F.; Baschnagel, J.  
594 Shear modulus of simulated glass-forming model systems: Effects of  
595 boundary condition, temperature, and sampling time. *J. Chem. Phys.*  
596 **2013**, *138*, 12A533. 597
- (42) Johnston, M. T.; Ewoldt, R. H. Precision rheometry: Surface  
598 tension effects on low-torque measurements in rotational rheometers. *J.*  
599 *Rheol.* **2013**, *57*, 1515–1532. 600
- (43) Napolitano, S.; Glynos, E.; Tito, N. B. Glass transition of  
601 polymers in bulk, confined geometries, and near interfaces. *Rep. Prog.*  
602 *Phys.* **2017**, *80*, 036602. 603
- (44) Napolitano, S.; Wübbenhorst, M. The lifetime of the deviations  
604 from bulk behaviour in polymers confined at the nanoscale. *Nat.*  
605 *Commun.* **2011**, *2*, 260. 606
- (45) George, G.; Kriuchevskiy, I.; Meyer, H.; Baschnagel, J.; Wittmer,  
607 J. P. Shear-stress relaxation in free-standing polymer films. *Phys. Rev. E:*  
608 *Stat. Phys., Plasmas, Fluids, Relat. Interdiscip. Top.* **2018**, *98*, 062502. 609
- (46) Bonn, D.; Eggers, J.; Indekeu, J.; Meunier, J.; Rolley, E. Wetting  
610 and spreading. *Rev. Mod. Phys.* **2009**, *81*, 739–805. 611
- (47) Graziano, R.; Preziosi, V.; Uva, D.; Tomaiuolo, G.; Mohebbi, B.;  
612 Claussen, J.; Guido, S. The microstructure of Carbopol in water under  
613 static and flow conditions and its effect on the yield stress. *J. Colloid*  
614 *Interface Sci.* **2021**, *582*, 1067–1074. 615
- (48) Conchúir, B. O.; Zacccone, A. Mechanism of flow-induced  
616 biomolecular and colloidal aggregate breakup. *Phys. Rev. E* **2013**, *87*,  
617 032310. 618
- (49) Matthews, H. K.; Ganguli, S.; Plak, K.; Taubenberger, A. V.; Win,  
619 Z.; Williamson, M.; Piel, M.; Guck, J.; Baum, B. Oncogenic Signaling  
620 Alters Cell Shape and Mechanics to Facilitate Cell Division under  
621 Confinement. *Dev. Cell* **2020**, *52*, 563–573. 622
- (50) Elder, R. M.; Knorr, D. B.; Andzelm, J. W.; Lenhart, J. L.; Sirk, T.  
623 W. Nanovoid formation and mechanics: a comparison of poly-  
624 (dicyclopentadiene) and epoxy networks from molecular dynamics  
625 simulations. *Soft Matter* **2016**, *12*, 4418–4434. 626
- (51) Miccio, L.; Cimmino, F.; Kurelac, I.; Villone, M. M.; Bianco, V.;  
627 Memmolo, P.; Merola, F.; Mugnano, M.; Capasso, M.; Iolascon, A.;  
628 Maffettone, P. L.; Ferraro, P. Perspectives on liquid biopsy for label-free  
629 detection of “circulating tumor cells” through intelligent lab-on-chips. *View*  
630 **2020**, *1*, 20200034. 631
- (52) Lv, P.; Yang, Z.; Hua, Z.; Li, M.; Lin, M.; Dong, Z. Measurement  
632 of viscosity of liquid in micro-crevice. *Flow Meas. Instrum.* **2015**, *46*,  
633 72–79. 634
- (53) Cheng, B.; Frenkel, D. Computing the Heat Conductivity of  
635 Fluids from Density Fluctuations. *Phys. Rev. Lett.* **2020**, *125*, 130602. 636
- (54) Jung, G.; Petersen, C. F. Confinement-induced demixing and  
637 crystallization. *Phys. Rev. Research* **2020**, *2*, 033207. 638

- 640 (55) Kume, E.; Baroni, P.; Noirez, L. Strain-induced violation of  
641 temperature uniformity in mesoscale liquids. *Sci. Rep.* **2020**, *10*, 13340.
- 642 (56) Do, J.-L.; Friščić, T. Mechanochemistry: A Force of Synthesis.  
643 *ACS Cent. Sci.* **2017**, *3*, 13–19.
- 644 (57) Howard, J. L.; Cao, Q.; Browne, D. L. Mechanochemistry as an  
645 emerging tool for molecular synthesis: what can it offer? *Chem. Sci.*  
646 **2018**, *9*, 3080–3094.
- 647 (58) van Galen, M.; van der Gucht, J.; Sprakel, J. Chemical Design  
648 Model for Emergent Synthetic Catch Bonds. *Front. Phys.* **2020**, *8*, 361.
- 649 (59) Klein, I. M.; Husic, C. C.; Kovács, D. P.; Choquette, N. J.; Robb,  
650 M. J. Validation of the CoGEF Method as a Predictive Tool for Polymer  
651 Mechanochemistry. *J. Am. Chem. Soc.* **2020**, *142*, 16364–16381.
- 652 (60) Michels, L.; Gorelova, V.; Harnvanichvech, Y.; Borst, J. W.;  
653 Albada, B.; Weijers, D.; Sprakel, J. Complete microviscosity maps of  
654 living plant cells and tissues with a toolbox of targeting mechanoprobes.  
655 *Proc. Natl. Acad. Sci. U. S. A.* **2020**, *117*, 18110–18118.
- 656 (61) Hickenboth, C. R.; Moore, J. S.; White, S. R.; Sottos, N. R.;  
657 Baudry, J.; Wilson, S. R. Biasing reaction pathways with mechanical  
658 force. *Nature* **2007**, *446*, 423–427.
- 659 (62) Konda, S. S. M.; Brantley, J. N.; Bielawski, C. W.; Makarov, D. E.  
660 Chemical reactions modulated by mechanical stress: Extended Bell  
661 theory. *J. Chem. Phys.* **2011**, *135*, 164103.
- 662 (63) Konda, S. S. M.; Avdoshenko, S. M.; Makarov, D. E. Exploring  
663 the topography of the stress-modified energy landscapes of  
664 mechanosensitive molecules. *J. Chem. Phys.* **2014**, *140*, 104114.
- 665 (64) Roessler, A. G.; Zimmerman, P. M. Examining the Ways To Bend  
666 and Break Reaction Pathways Using Mechanochemistry. *J. Phys. Chem.*  
667 *C* **2018**, *122*, 6996–7004.